DOI: 10.1478/AAPP.1032A3

AAPP | Atti della Accademia Peloritana dei Pericolanti
Classe di Scienze Fisiche, Matematiche e Naturali
ISSN 1825-1242

Vol. 103, No. 2, A3 (2025)

NATURAL RADIOACTIVITY CONTENT, RADON EXHALATION AND MINERALOGICAL COMPOSITION ASSESSMENT OF THE IGNIMBRITE CAMPANA STONE: A CASE STUDY

FRANCESCO CARIDI [a*], DANIELE CHIRIU [b], STEFANIA DA PELO [c], GIULIANA FAGGIO [d], MICHELE GUIDA [e], GIACOMO MESSINA [d], MAURIZIO PONTE [f], SILVESTRO ANTONIO RUFFOLO [f], DOMENICO MAJOLINO [a] AND VALENTINA VENUTI [a]

ABSTRACT. The natural radioactivity content of the *Ignimbrite campana* stone, as well as its radon exhalation and mineralogical composition, were assessed and reported as a case study in the present paper. In particular, the High Purity Germanium (HPGe) gamma spectrometry and the Closed Chamber Method (CCM) with the Durridge Rad7 setup were employed to quantify the specific activities of ^{226}Ra, ^{232}Th and ^{40}K, and the radon exhalation rate, respectively. In addition, several indexes were calculated to evaluate the radiological health risk related to radiation exposure from the analyzed natural stone, i.e. the absorbed gamma dose rate (D), the annual effective dose equivalent (AEDE), the activity concentration index (I), and the alpha index (I_α). Finally, X-Ray Diffraction (XRD) and Micro-Raman Scattering (MRS) investigations were performed to correlate the chemical composition and mineralogical characteristics of the investigated natural stone with its natural radioactivity content and radon exhalation rate.

1. Introduction

Natural background radiation accounts for the majority of the global population's external dose (United Nations Scientific Committee on the Effects of Atomic Radiation 2000). Natural sources of ^{238}U, ^{232}Th, and ^{40}K include soil, sand, and rocks. The abundance and distribution of these radionuclides depend on the local geology of each region of the world (Navas, Soto, and Machín 2002). Natural materials used in dwellings can emit gamma radiation in both indoor and outdoor environments, and the prolonged exposure to low amounts of radiation can harm human health (Caridi *et al.* 2021). Thus, evaluating the concentration of radiation emitters in natural building materials (BM) used in dwellings is important as people spend the majority of their time indoors (Torrisi *et al.* 2008; Omar-Nazir *et al.* 2018).

The European Union (EU) has established a series of regulations and directives since 1989 with the objective of regulating the radiation emitted from building materials, taking

into account the potential health effects of radiation exposure in indoor environments. In particular, in 1999, the European Commission (EC) announced the ALARA (As Low As Reasonably Achievable) principle and established the limitation of radiation exposure from substances with high levels of naturally occurring radionuclides as the ultimate goal of radiation control in building materials (EC Radiation Protection 1999). In order to achieve this objective, the EC initially introduced the radiation activity concentration index (I), which is typically employed as a screening tool to restrict gamma radiation exposure of construction materials (Righi and Bruzzi 2006). Furthermore, several additional indexes have been devised over time for the purpose of evaluating the radiological risk associated with radiation exposure from such samples (Caridi, Messina, and D'Agostino 2017; Caridi *et al.* 2023). In more recent times, the radiological concerns regarding public health have been subjected to careful consideration by the EU in the European Directive 2013/59 EURATOM, which has been translated into the Italian legislation as D. Lgs. 101/2020. In particular, the directive emphasises the importance of investigating all potential sources of indoor radon, including soil, building materials, water and natural gas provided by domestic plants. This is to achieve increasingly biocompatible housing from a radiological perspective. In light of these considerations, it is unsurprising that public concern about radon exhalation from building materials and its contribution to indoor radon levels is on the rise. This is particularly so in the context of radiation protection from radon gas exposure (Mancini *et al.* 2017). In this context, the PRIN 2022 PNRR ATHENA (A novel approach towards the management of building materials of particular historical-artistic interest: assessment of the radon exhalation and the radiological risk due to natural radioactivity content) project, funded by the European Union - Next Generation EU, provides the context for the development of this paper. The project is focused on the systematic implementation of novel operative strategies for the evaluation of the radon exhalation rate in building materials. This rate, defined as the rate of radon escaping into the atmosphere, is crucial for the comprehensive evaluation of the radiological health risk associated with radon exposure in indoor environments. It is noteworthy that studies aimed at assessing the natural radioactivity content in building materials, as well as monitoring the radon concentration in indoor environments, are widely documented in the literature (Stoulos, Manolopoulou, and Papastefanou 2003; Chen, Moir, and Whyte 2012). Nevertheless, only a limited amount of data is currently available concerning the natural radioactivity content of stone materials employed in the construction of buildings of historical and artistic significance, including churches, monuments, and other edifices. Additionally, there is a lack of information regarding the natural radioactivity content of stone materials used in structural applications, such as paving stones, columns, and flooring. Indeed, in this particular context of unique and highly vulnerable masterpieces, the identification and investigation of sources of radiation exhalation is more challenging than in more modern conventional buildings. It thus follows that the development of appropriate techniques and protocols for the quantitative evaluation of the activity concentrations of ^{226}Ra, ^{232}Th and ^{40}K, together with the radon release in construction materials, can play a fundamental role in the field of cultural heritage. This is particularly relevant given that materials potentially enriched with naturally occurring radionuclides (and thus with radon) have been used in the past to build historical-artistic monuments. Therefore, this could represent a significant health concern for inhabitants, visitors and workers, particularly in the context of underground archaeological sites, crypts

and catacombs. Such knowledge is of particular importance in Italy, which has the most numerous and fascinating archaeological sites in the world, according to the United Nations Educational, Scientific and Cultural Organization (UNESCO) World Heritage Sites.

In this paper, we assess and report the radon exhalation from the *Ignimbrite campana* (CI) building material, as well as its natural radioactivity content and the radiological health risk for humans through the calculation of the absorbed gamma dose rate (D), the annual effective dose equivalent (AEDE), the activity concentration index (I), and the alpha index (I_α), as a case study. In addition, X-ray diffraction (XRD) and micro-Raman scattering (MRS) investigations were conducted to establish a correlation between the chemical composition and mineralogical characteristics of the investigated natural stone and its natural radioactivity content and radon exhalation rate.

2. Geological framework

Caldera-forming eruptions are one of the most hazardous natural events on Earth. *Ignimbrite campana* represents a classical example of such events, producing a voluminous pyroclastic sequence of trachytic to phonolitic magma that covered several thousands of squared kilometers in the Campanian Plain, (Campania, south-central Italy), around 39 ka ago (Forni *et al.* 2016). The structure of the Campanian Plain is characterized by upper Miocene thrusts of the southern Apennines displaced by numerous Quaternary fault systems associated with the final stages of the opening of the Tyrrhenian Sea. Analyses of the structural highs and downthrown zones of the Campanian margin show that NW-SE normal faults of lower Pleistocene age predate NE-SW faults of post-700 ka age. The Late Quaternary fault pattern of the Bay of Naples is characterized by E-W trending left-lateral faults, NE trending normal faults and NW trending transtensional faults, probably as the result of block rotation associated with a transtensional regime along an E-W left-lateral fault zone.

In the last 600 ka, the Campanian volcanic zone (CVZ) has been affected by uplift and intense volcanism, alternating with periods of subsidence and marine sedimentation. Volcanological studies indicate that at least five ignimbrites were emplaced over the CVZ in the last 300 ka, and no caldera structure has been recognized associated with this ignimbrite volcanism. The trachytic ignimbrites are dated at 290 ka and 240 ka (Seiano Ignimbrites), 157 ka (Taurano Ignimbrite), 116 ka (Durazzano Ignimbrite), and 39 ka (CI units). Approximately 36000 years ago the area presently occupied by the Phlegraean Fields was the site of one of the world's of trachytic magma was explosively erupted as pumice and ash, resulting in the deposition of subaerial plinian fallout deposit and ash-flow tuff over a large part of southern Italy, and volcanigenic marine sediments (ash fallout deposits and turbidites). The principal deposit is a welded to sintered ignimbrite formerly designated the Campanian Grey Tuff, but presently called *Ignimbrite campana*. The eruption products that have shaped the current morphology of the Campanian Plain are those of the last two major eruptions, the 39 ka CI unit-1 and the 15 ka (Neapolitan Yellow Tuff). The volcano that erupted the NYT, forming the Campi Flegrei caldera, is well preserved in the northern sector. It juts into Campanian Plain covering both the ignimbritic units of 39 ka with a layer of loose pyroclastic products (Pozzolana) (Deino *et al.* 2004). The CI is a voluminous and widespread pyroclastic sequence composed of a basal fallout deposit and distinct pyroclastic

flow units. The lithology and depositional characteristics (lithofacies) of the CI change both laterally and vertically, especially due to variations in emplacement mechanisms, degree of welding and post-depositional processes.

This gives origin to the superposition of different units, with different areal distribution and large variability from proximal to distal sites. Along and close to the caldera rims, the CI deposits occur in scattered outcrops mainly representing the proximal facies of this formation. Some authors have called these deposits the "Breccia Museo sequence" identifying six stratigraphic units, which also include the usually distal lapilli fall basal layers. From the bottom to the top, this sequence is composed of: 1) plinian pumice fall deposit (PPF); 2) unconsolidated stratified ash flow (USAF); 3) welded grey ignimbrite (WGI); 4) lower pumice flow unit (LPFU); 5) coarse lithic breccia (BU) sometimes interlayered with welded spatter beds (SU); 6) upper pumice flow unit (UPFU) (Forni *et al.* 2016).

The sample of this study came from (Quarto) Napoli and, from a geological point of view belong to CI (Forni *et al.* 2016). The facies of CI are exposed at the northern and southern foot of Camaldoli Hill, at Pianura and Soccavo (Torre Franco and Verdolino). The only documented quarries are located in the above-cited areas of Campi Flegrei and are formed by tunnels branching under the hill. The formation seems to gently dip northward, but its base is not exposed; however, whenever visible, thickness is about 20 m (Calcaterra *et al.* 2004).

3. Materials and methods

Five aliquots of the investigated *Ignimbrite campana* natural stone were obtained by cutting at the laboratory larger pieces of stones by means of a circular saw. Each aliquot was a cube of approximately 5 cm as side.

3.1. HPGe gamma spectrometry analysis. Prior to analysis by HPGe gamma spectrometry, each aliquot of the investigated sample was first pulverised and then subjected to a 24-hour drying process at 105 °C in an oven, with the objective of completely removing moisture. Subsequently, each aliquot was sieved in order to obtain a particle size of less than 2 mm and was then placed in Marinelli sealed containers of 1 L capacity. Subsequently, the sample was left for 30 days to allow for secular equilibrium between ^{226}Ra and its daughter products to be reached. Furthermore, to reduce the statistical uncertainty, a total acquisition time of 70000 seconds was employed, and the spectra were analysed in order to quantify the activity concentration of ^{226}Ra, ^{232}Th, and ^{40}K. Specifically, the 351.92 keV ^{214}Pb and 1120.29 keV ^{214}Bi gamma-ray lines were employed to quantify the ^{226}Ra activity concentration; the 911.21 keV ^{228}Ac gamma-ray line was used to assess the ^{232}Th specific activity; the 1460.8 keV gamma-ray line was used to evaluate the activity concentration of ^{40}K. The experimental setup comprises a negative-biased detector (GMX) Ortec HPGe detector and integrated digital electronics. The detector is cooled by the Ortec recycler condensing liquid nitrogen cooling Mobius system, and it is characterized by a full width at half maximum (FWHM) of 1.94 keV, a peak to Compton ratio of 65:1 and a relative efficiency of 37.5% at 1.33 MeV (^{60}Co). The Eckert and Zigler Nuclitec GmgH traceable multinuclide radioactive standard, number AK-5901, with an energy range 59.54 keV-1836 keV, was employed to perform efficiency and energy calibrations. This standard reproduces the exact samples geometries in a water-equivalent epoxy resin matrix. The data acquisition

and subsequent analysis were conducted using the Gamma Vision software, developed by Ortec. The specific activity (Bq kg^{-1} dry weight, d.w.) of the investigated radioisotopes was calculated using the following formula (Caridi *et al.* 2017b):

$$C\,(\mathrm{Bq\,kg^{-1}\ dry\ weight}) = \frac{N_E}{\varepsilon_E\, t\, \gamma_d\, M} \tag{1}$$

where N_E, ε_E and γ_d account for the net area, the efficiency and yield of a photopeak at energy E, respectively; M is the dry mass of the sample (kg) and t is the acquisition time (s). The measurement error, given at the 95% confidence level, was determined by considering the following components: uncertainty of the counting estimation, of the calibration source, of the efficiency calibration, of the background subtraction and of the γ-branching ratio (Caridi *et al.* 2019). The quality of the HPGe gamma spectrometry results was certified by the Italian Accreditation Body (ACCREDIA) on the basis of the quality controls performed in accordance with the UNI 11665:2017 standard.

3.2. Evaluatuion of the radiological health risk.

3.2.1. *Absorbed gamma dose rate (D).* The absorbed gamma dose rate, D (nGy h^{-1}), was initially employed to quantify the radiological health risk associated with indoor external exposure. The aforementioned rate was calculated using the standard room model, as previously stated by Caridi *et al.* (2017a):

$$D = 0.92C_{\mathrm{Ra}} + 1.1C_{\mathrm{Th}} + 0.08C_{\mathrm{K}} \tag{2}$$

where C_{Ra}, C_{Th} and C_{K} are the average activity concentrations (the mean value of the five analyzed aliquots) of ^{226}Ra, ^{232}Th, and ^{40}K in the analyzed sample, respectively.

3.2.2. *Annual Effective Dose Equivalent.* In the event of an 80% employment factor for indoor exposure, the annual effective dose equivalent (AEDE) (mSv y^{-1}) of an individual may be calculated as follows (Dattola *et al.* 2024):

$$AEDE = (D-50) \times 8760h \times 0.7\,Sv\,Gy^{-1} \times 0.8 \times 10^{-6} \tag{3}$$

where the average dose rate value of 50 nGy h^{-1} for the background was discounted. In order for a radiological danger to be considered minimal, AEDE must be less than 1 mSv y^{-1} (Caridi *et al.* 2016).

3.2.3. *Activity Concentration Index.* In order to ascertain whether the dose criterion is satisfied, the European Commission has established an activity concentration index (I) (Caridi *et al.* 2023):

$$I = C_{\mathrm{Ra}}/300 + C_{\mathrm{Th}}/200 + C_{\mathrm{K}}/3000 \tag{4}$$

This is in reference to the established limit of 1 mSv y^{-1}, which applies to exposure to gamma radiation emitted by building materials (AEDE), in addition to outdoor exposure (Alghamdi, Aleissa, and Al-Hamarneh 2019). Consequently, the purpose of this index would be to serve as a screening tool for identifying materials that may pose a risk when used in buildings. It is advisable to refrain from those with $I > 1$, as these values indicate exposure rates more than 1 mSv y^{-1}.

3.2.4. *Alpha Index.* The alpha index was calculated as follows (Dattola *et al.* 2024):

$$I_\alpha = \frac{C_{\mathrm{Ra}}}{200} \tag{5}$$

It provides an indication of the alpha radiation exposure resulting from the indoor radon exhaled from building materials. In order to prevent exposure to indoor radon specific activity in excess of the threshold value of 200 Bq m^{-3}, the activity concentration of ^{226}Ra must be less than 200 Bq kg^{-1}. Furthermore, in order to ensure a minimal risk of exposure to radiation, I_α must be less than 1 (Caridi *et al.* 2023).

3.3. Radon exhalation rate measurements. The radon exhalation rate of each aliquot of the investigated natural stone was determined by employing the Closed Chamber Method (CCM) (Tuccimei *et al.* 2015). In particular, the experimental apparatus comprises a small cylindrical steel vessel (volume 2.75 L) connected to the Durridge Rad7 instrument, a desiccant ($CaSO_4$) and some vinyl tubes forming a closed circuit (Alhamdi and Abdullah 2021).

The air within the chamber, following its passage through the drying unit and inlet filter, is drawn into the instrument, reaching its measuring chamber, and subsequently returned to the stainless-steel chamber through the outlet filter (output), thus forming a closed loop. As the filtered air decays within the chamber, it produces alpha-emitting progeny, particularly polonium isotopes, which can be detected. A high voltage of 2500 V is applied to the chamber walls. The Rad7 solid-state silicon detector converts alpha radiation directly to an electrical signal, differentiating between the electrical pulses generated by α-particles and those generated by ^{218}Po, ^{216}Po, ^{214}Po and ^{212}Po, with energies of 6 MeV, 6.7 MeV, 7.7 MeV and 8.8 MeV, respectively. This approach allows the use of the ^{218}Po peak for ^{222}Rn, facilitating rapid equilibrium between polonium and radon nuclei. This is because equilibrium between ^{218}Po and ^{222}Rn is achieved in approximately 15 minutes, which is approximately five times the half-life of ^{218}Po (Tuccimei, Moroni, and Norcia 2006). The radon growth curve to equilibrium was monitored over a period of 10 days, and the ^{222}Rn specific exhalation rate (E, in Bq h^{-1} kg^{-1}) was calculated according to the following equation (Tuccimei, Moroni, and Norcia 2006):

$$E = \frac{(C - C_0 e^{-\lambda T})/m}{1 - e^{-\lambda T}} \lambda V \tag{6}$$

In this context, C represents the equilibrium concentration (Bq m^{-3}), C_0 denotes the initial radon concentration (Bq m^{-3}), λ (h^{-1}) indicates the sum of the radon decay constant, the bound exhalation constant and the leakage constant, V stands for the total volume of the analytical system (m^3), T is the time of exposure (h) and m is the mass of the sample (kg). In order to minimise the leakage from the chamber, an insulating rubber was utilised.

3.4. X-Ray Diffraction (XRD) setup. X-ray diffraction analyses were conducted using a Panalytical Empyrean Diffractometer, equipped with Cu K_α radiation and a Bragg–Brentano theta–theta goniometer, utilising a solid-state PIXcel detector. Approximately 1 g of the finely powdered sample of natural stone was employed for each analysis. The acquisition settings were 40 kV and 40 mA, with XRD patterns recorded over a 2θ range from 2° to

70°, employing a step size of 0.007° and a counting time of 20 seconds. To eliminate the Cu $K_{\alpha 2}$ component, the initial data were processed using software correction, while the background was corrected using a digital filter. The observed peak positions were then compared against the ICDD JCPDS database in order to identify the crystalline mineral components present in the analysed natural stone (Morelli *et al.* 2012).

3.5. Micro-Raman scattering (MRS) measurements. Micro-Raman scattering (MRS) measurements were conducted on the stone under investigation using a portable spectrometer, the BTR111MiniRa^{TM}, manufactured by BW&TEK Inc. The instrument employs a 785 nm (diode laser) excitation wavelength and a thermoelectric cooled charge-coupled device (CCD) detector. The system was equipped with a BAC151B Raman microscope. The laser beam was focused on the surface through a $40\times$ / $80\times$ objective, ensuring a working distance of 3.98 mm and a laser beam spot size of $50/25$ μ m. In this instance, the maximum laser power applied to the samples was approximately 90 mW. The spectra were recorded within a wavenumber range of 60 to 3150 cm^{-1}, with an acquisition time of 10 seconds and a resolution of 8 cm^{-1}. In order to enhance the signal-to-noise ratio, 18 scans were accumulated. Prior to each measurement, a calibration procedure was conducted to ensure the optimal performance of the instrument, utilising the peak at 520.6 cm^{-1} of a silicon chip as a reference point (Caridi *et al.* 2022).

4. Results and discussion

4.1. Activity concentration and radon exhalation rate. The average ^{226}Ra, ^{232}Th and ^{40}K activity concentrations and ^{222}Rn exhalation rate (the mean value of the five analyzed aliquots), for the analyzed natural stone, are reported in Table 1.

TABLE 1. The average ^{226}Ra, ^{232}Th and ^{40}K activity concentrations and ^{222}Rn exhalation rate for the *Ignimbrite campana* stone.

Sample	Specific activity			^{222}Rn exhalation rate
	C_{Ra} (Bq kg^{-1} d.w.)	C_{Th} (Bq kg^{-1} d.w.)	C_K (Bq kg^{-1} d.w.)	(Bq h^{-1} kg^{-1})
Ignimbrite campana	104 ± 16	121 ± 18	1879 ± 214	0.080 ± 0.010

First of all, it is worth remarking that these findings are consistent with the natural radioactive levels observed in similar building materials used in Italy (Sabbarese *et al.* 2021; Ambrosino *et al.* 2024). In particular, as far as the natural radioactivity content is concerned, it is important to point out that the specific activities of ^{226}Ra, ^{232}Th and ^{40}K, as well as ^{222}Rn exhalation rate, are significantly higher than the average world values (United Nations Scientific Committee on the Effects of Atomic Radiation 2000). Published research indicates that the chemical composition and mineralogical characteristics of natural stones exert a considerable influence on the values of the ^{222}Rn exhalation rate, as well as those of C_{Ra}, C_{Th}, and C_K (Avwiri, Egieya, and Ononugbo 2013). In light of these findings, further investigations were conducted to ascertain the chemical and mineralogical composition of

the *Ignimbrite campana* stone. These investigations employed micro-Raman scattering and X-ray diffraction techniques, the results of which are detailed in the following. Moreover, as far as the radon exhalation rate from the analyzed natural stone is concerned, it is worth noting that the obtained value aligned well with worldwide measurements (Girault *et al.* 2011; Gruber *et al.* 2013).

4.2. Radiological health risk assessment. The absorbed gamma dose rate (D), the annual effective dose equivalent (AEDE), the activity concentration index (I) and the alpha index (I_α), as calculated using the equations provided in (2-5), are presented in Table 2.

TABLE 2. The absorbed gamma dose rate (D), the annual effective dose equivalent (AEDE), the activity concentration index (I) and the alpha index (I_α) for the investigated sample.

Sample	D (nGy h^{-1})	AEDE (mSv y^{-1})	I	I_α
Ignimbrite campana	379	1.6	1.6	0.5

In particular, the D value of 379 nGy h^{-1} can be attributed to the lithological component of the sample under investigation (Pietrzak and McPhail 2004) and was used to calculate AEDE through Eq. (3). Noteworthy, in the extremely precautionary scenario assumed (8760 hours of exposure, i.e. 24 hours a day for 365 days), the latter was found to be 1.6 mSv y^{-1}, which is higher than the action level of 1 mSv y^{-1} reported by the Italian legislation for members of the population (Legislation 2020). Furthermore, the I index was found to be 1.6, higher than the threshold value of 1. These results impose, for the purposes of using this natural stone for civil engineering buildings, such as dwellings and buildings with a high occupancy factor, a more accurate assessment of the dose in accordance with Article 29, Paragraph 5, of D. Lgs. 101/20, applying dose estimation methods provided by national and international standards that take into account other factors, including density, material thickness, as well as factors relating to the type of building and the intended use of the material (structural or surface) (European Commission and Directorate-General for Environment 2000). Finally, I_α was found to be 0.5, which is below the threshold value, thus rationally ruling out any significant health impact from exposure to radon gas exhaled by the investigated natural stone.

4.3. XRD analysis. The most representative XRD spectrum for the *Ignimbrite campana* stone is shown in Fig. 1. It reveals multiple crystalline phases: biotite (Bt), diopside (Dps), analcime (Anc) and albite (Alb) (Deer, Howie, and Zussman 2013). Biotite is identified by peaks around $2\theta = 8^\circ, 13^\circ, 23^\circ, 28^\circ$, while diopside peaks are present at approximately $2\theta = 10^\circ, 23^\circ, 32^\circ, 36^\circ, 50^\circ, 54^\circ, 58^\circ, 62^\circ$. Analcime shows peaks around $2\theta = 18^\circ, 22^\circ$ and albite at $2\theta = 27^\circ, 30^\circ, 38^\circ, 44^\circ, 48^\circ$ (Bish and Plötze 2010). The sharpness of these peaks indicates a well-crystallized structure, suggesting minimal alteration or weathering of the minerals. The identification of these phases is consistent with the mineralogical composition typical of ignimbrites, which are volcanic rocks formed from pyroclastic flows (Jenkins and Snyder 1996).

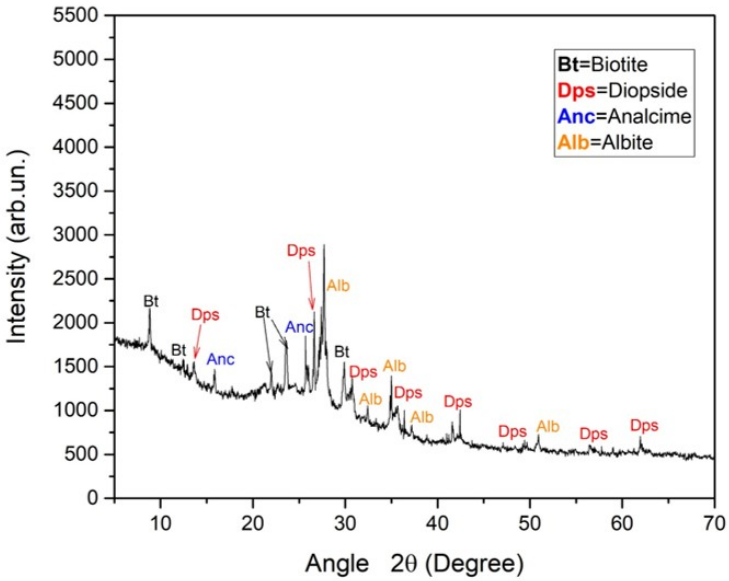

FIGURE 1. XRD pattern of *Ignimbrite campana* specimen.

The combination of biotite, diopside, analcime and albite points to a complex formation history involving high-temperature conditions and subsequent hydrothermal alterations (Rollog *et al.* 2019). Biotite and diopside indicate the presence of potassium and trace amounts of uranium and thorium, contributing to the natural radionuclide content. Analcime suggests secondary processes involving zeolite formation, while albite reflects the feldspathic nature of the *Ignimbrite campana* (Rodrigues e Silva and Monteiro de Oliveira 2023). The presence of these minerals plays a key role in understanding the petrogenesis of the *Ignimbrite campana* and its thermal history. Biotite, in particular, is a source of ^{40}K (Carvalho *et al.* 2021). Diopside and albite can contain trace amounts of uranium and thorium, further contributing to the radioactivity levels (Sabol and Weng 1995).

The XRD analysis of the *Ignimbrite campana* confirms a heterogeneous mineralogical composition, with biotite, diopside, analcime and albite being the primary phases. The well-crystallized nature of these minerals suggests high purity, with significant implications for the natural radionuclide content. This composition provides insights into the geological history and formation processes of this natural stone.

4.4. MRS analysis. Figure 2 shows the obtained micro-Raman spectra collected on different spots of the *Ignimbrite campana* stone, which furnished evidence of a complex molecular composition characterized by the co-existence of different chemical species.

Concerning spot S1 (Fig. 2a), related to a black area of the analyzed surface, the detected μ-Raman profile revealed a composition based on diopside, with bands at ~ 323 cm^{-1} (m), ~ 386 cm^{-1} (m), ~ 559 cm^{-1} (w), ~ 666 cm^{-1} (m-s), and ~ 1002 cm^{-1} (s).

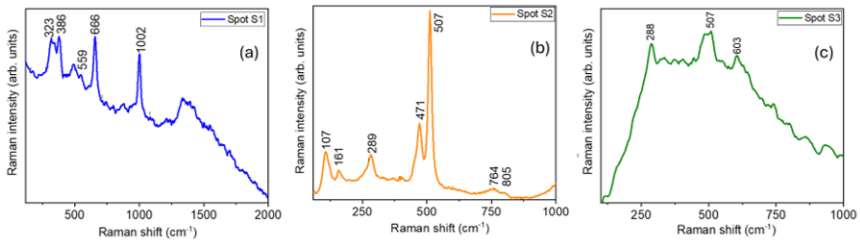

FIGURE 2. Representative micro-Raman spectra recorded on three different spots of the *Ignimbrite campana* stone.

The μ-Raman spectrum collected on a light grey area (Fig. 2b) holds all the main vibrational features associated to albite, with features falling at $\sim 107\,\mathrm{cm}^{-1}$ (m), $\sim 161\,\mathrm{cm}^{-1}$ (w), $\sim 289\,\mathrm{cm}^{-1}$ (m), $\sim 471\,\mathrm{cm}^{-1}$ (m-s), $\sim 507\,\mathrm{cm}^{-1}$ (s), $\sim 764\,\mathrm{cm}^{-1}$ (br) and $\sim 805\,\mathrm{cm}^{-1}$ (br).

Finally, the observation of three contributions centered at $\sim 289\,\mathrm{cm}^{-1}$, $\sim 507\,\mathrm{cm}^{-1}$ and $\sim 603\,\mathrm{cm}^{-1}$ (see Fig. 2c) in the μ-Raman spectrum collected from a dark orange spot (spot 3) of the surface can be ascribed to the presence of analcime mineral in the investigated stone. The observed molecular composition is in agreement with the mineralogical phases attained through XRD.

5. Conclusions

Natural radioactivity content, radon exhalation rate and mineralogy of a natural stone of particular historical and artistic interest employed as building material, i.e. the *Ignimbrite campana* stone, were investigated through a multidisciplinary approach, by using the High Purity Germanium (HPGe) gamma-ray spectrometry, the Closed Chamber Method (CCM) with the Durridge Rad7 apparatus for short-lived radon progeny alpha spectrometry, the X-ray diffraction (XRD) and the Micro-Raman Scattering (MRS) spectroscopy.

In particular, the activity concentrations of ^{226}Ra, ^{232}Th and ^{40}K, as well as ^{222}Rn exhalation rate, were found to be higher than the average global values. Furthermore, in order to evaluate the potential radiological risks associated with radiation exposure from the analysed specimen, the absorbed gamma dose rate, the annual effective dose equivalent, the activity concentration index, and the alpha index were estimated. In particular, in the extremely precautionary scenario assumed, the AEDE value was found to be higher than the action threshold specified by Italian legislation for the public, namely $1\,\mathrm{mSv\,y}^{-1}$. Moreover, the I index was found to be higher than the threshold value of 1. These results impose, for the purposes of using this natural stone for civil engineering buildings, such as dwellings and buildings with a high occupancy factor, a more accurate assessment of the dose in accordance with Article 29, Paragraph 5, of D. Lgs. 101/20. Furthermore, it was verified that I_α was less than unity, indicating that the radiological risks associated with exposure to indoor radon concentrations exceeding $200\,\mathrm{Bq\,m}^{-3}$ is extremely low.

Ultimately, the presence of biotite, diopside, analcime and albite as main predominant minerals was confirmed through the utilisation of XRD and micro-Raman spectroscopy. In

detail, biotite is a source of ^{40}K, while diopside and albite can contain trace amounts of uranium and thorium, further contributing to the radioactivity levels.

Funding

This work was performed in the framework of the PRIN 2022 PNRR ATHENA (A novel approach Towards the management of building materials of particular Historical-artistic interest: assessment of the radon Exhalation and the radiological risk due to Natural radioActivity content) project, CUP J53D23014560001, funded by the European Union - Next Generation EU, PNRR - Mission 4, Component 2, Investment 1.1 - PRIN 2022 PNRR Call for Proposals - Directorial Decree No. 1409 of 14-09-2022.

References

Alghamdi, A. S., Aleissa, K. A., and Al-Hamarneh, I. F. (2019). "Gamma radiation and indoor radon concentrations in the western and southwestern regions of Saudi Arabia". *Heliyon* **5**(1), e01133. DOI: 10.1016/j.heliyon.2019.e01133.

Alhamdi, W. A. and Abdullah, K. M. S. (2021). "Determination of radium and radon exhalation rate as a function of soil depth of Duhok Province - Iraq". *Journal of Radiation Research and Applied Sciences* **14**, 486–494. DOI: 10.1080/16878507.2021.1999719.

Ambrosino, F., La Verde, G., Gagliardo, G., Mottareale, R., Della Peruta, G., Imparato, C., D'Elia, A., and Pugliese, M. (2024). "Radon exhalation rate: A metrological approach for radiation protection". *Sensors* **24**, 3633. DOI: 10.3390/s24113633.

Avwiri, G. O., Egieya, J. M., and Ononugbo, C. P. (2013). "Radiometric assay of hazard indices and excess lifetime cancer risk due to natural radioactivity in soil profile in Ogba/Egbema/Ndoni local government area of Rivers State, Nigeria". *Academic Research International* **4**(5), 54–65. URL: http://www.savap.org.pk/journals/ARInt./Vol.4(5)/2013(4.5-07).pdf.

Bish, D. L. and Plötze, M. (2010). "X-Ray Powder Diffraction with Emphasis on Qualitative and Quantitative Analysis in Industrial Mineralogy". In: *Advances in the Characterization of Industrial Minerals*. Ed. by G. E. Christidis. Vol. 9. European Mineralogical Union Notes in Mineralogy. EMU and Mineralogical Society of the United Kingdom and Ireland. Chap. 3, pp. 35–76. DOI: 10.1180/emu-notes.2010.emu9-3.

Calcaterra, D., Cappelletti, P., Langella, A., Colella, A., and de Gennaro, M. (2004). "The ornamental stones of Caserta province: the Campanian Ignimbrite in the medieval architecture of Casertavecchia". *Journal of Cultural Heritage* **5**(2), 137–148. DOI: 10.1016/j.culher.2003.08.003.

Caridi, F., D'Agostino, M., Messina, M., Marcianò, G., Grioli, L., Belvedere, A., Marguccio, S., and Belmusto, G. (2017a). "Lichens as environmental risk detectors". *The European Physical Journal Plus* **132**, 189. DOI: 10.1140/epjp/i2017-11459-y.

Caridi, F., Di Bella, M., Sabatino, G., Belmusto, G., Fede, M. R., Romano, D., Italiano, F., and Mottese, A. F. (2021). "Assessment of natural radioactivity and radiological risks in river sediments from Calabria (Southern Italy)". *Applied Sciences* **11**(4), 1729. DOI: 10.3390/app11041729.

Caridi, F., Marguccio, S., D'Agostino, M., Belvedere, A., and Belmusto, G. (2016). "Natural radioactivity and metal contamination of river sediments in the Calabria region, south of Italy". *The European Physical Journal Plus* **131**, 155. DOI: 10.1140/epjp/i2016-16155-x.

Caridi, F., Marguccio, S., Durante, G., Trozzo, R., Fullone, F., Belvedere, A., D'Agostino, M., and Belmusto, G. (2017b). "Natural radioactivity measurements and dosimetric evaluations in soil samples with a high content of NORM". *The European Physical Journal Plus* **132**, 56. DOI: 10.1140/epjp/i2017-11343-x.

Caridi, F., Messina, M., Belvedere, A., D'Agostino, M., Marguccio, S., Settineri, L., and Belmusto, G. (2019). "Food salt characterization in terms of radioactivity and metals contamination". *Applied Sciences* **9**(14), 2882. DOI: 10.3390/app9142882.

Caridi, F., Messina, M., and D'Agostino, M. (2017). "An investigation about natural radioactivity, hydrochemistry, and metal pollution in groundwater from Calabrian selected areas, southern Italy". *Environmental Earth Sciences* **76**, 668. DOI: 10.1007/s12665-017-7031-9.

Caridi, F., Paladini, G., Marguccio, S., Belvedere, A., D'Agostino, M., Messina, M., Crupi, V., Venuti, V., and Majolino, D. (2023). "Evaluation of radioactivity and heavy metals content in a basalt aggregate for concrete from Sicily, Southern Italy: A case study". *Applied Sciences* **13**, 4804. DOI: 10.3390/app13084804.

Caridi, F., Spoto, S. E., Paladini, G., Venuti, V., Crupi, V., Ricca, M., and Majolino, D. (2022). "Natural radioactivity content and mineralogical composition of beach sands from the Gulf of Squillace, Southern Italy: A case study". *AAPP Atti della Accademia Peloritana dei Pericolanti. Classe di Scienze Fisiche Matematiche e Naturali* **100**(2), A11 [13 pages]. DOI: 10.1478/AAPP.1002A11.

Carvalho, F. P., Tufa, M. B., Oliveira, J. M., and Malta, M. (2021). "Radionuclides and radiation exposure in tantalite mining, Ethiopia". *Archives of Environmental Contamination and Toxicology* **81**(4), 648–659. DOI: 10.1007/s00244-021-00858-8.

Chen, J., Moir, D., and Whyte, J. (2012). "Canadian population risk of radon induced lung cancer: a re-assessment based on the recent cross-Canada radon survey". *Radiation Protection Dosimetry* **152** (1-3), 9–13. DOI: 10.1093/rpd/ncs147.

Dattola, L., Belvedere, A., D'Agostino, M., Faggio, G., Majolino, D., Marguccio, S., Messina, G., Messina, M., Mottese, A. F., Paladini, G., Venuti, V., and Caridi, F. (2024). "Assessment of the radioactivity, metals content and mineralogy of granodiorite from Calabria, Southern Italy: A case study". *Materials* **17**, 3813. DOI: 10.3390/ma17153813.

Deer, W. A., Howie, R. A., and Zussman, J. (2013). *An Introduction to the Rock-Forming Minerals*. 3rd ed. Mineralogical Society of the United Kingdom and Ireland. DOI: https://doi.org/10.1180/DHZ.

Deino, A. L., Orsi, G., de Vita, S., and Piochi, M. (2004). "The age of the Neapolitan Yellow Tuff caldera-forming eruption (Campi Flegrei caldera–Italy) assessed by $^{40}Ar/^{39}Ar$ dating method". *Journal of Volcanology and Geothermal Research* **133** (1-4), 157–170. DOI: 10.1016/S0377-0273(03)00396-2.

European Commission and Directorate-General for Environment (2000). *Radiological protection principles concerning the natural radioactivity of building materials*. Publications Office of the European Union. URL: https://op.europa.eu/en/publication-detail/-/publication/988f3243-5259-43a5-b621-fbff662deeb0/language-en.

Forni, F., Bachmann, O., Mollo, S., De Astis, G., Gelman, S. E., and Ellis, B. S. (2016). "The origin of a zoned ignimbrite: Insights into the Campanian Ignimbrite magma chamber (Campi Flegrei, Italy)". *Earth and Planetary Science Letters* **449**, 259–271. DOI: 10.1016/j.epsl.2016.06.003.

Girault, F., Gajurel, A. P., Perrier, F., Upreti, B. N., and Richon, P. (2011). "Radon emanation of heterogeneous basin deposits in Kathmandu Valley, Nepal". *Journal of Asian Earth Sciences* **40**, 595–610. DOI: 10.1016/j.jseaes.2010.10.012.

Gruber, V., Bossew, P., De Cort, M., and Tollefsen, T. (2013). "The European map of the geogenic radon potential". *Journal of Radiological Protection* **33**, 51. DOI: 10.1088/0952-4746/33/1/51.

Jenkins, R. and Snyder, R. L. (1996). "Introduction to X-Ray Powder Diffractometry". In: *Chemical Analysis: A Series of Monographs on Analytical Chemistry and Its Applications*. Ed. by J. D. Winefordner. Vol. 138. John Wiley & Sons, Ltd. DOI: 10.1002/9781118520994.fmatter.

Legislation (2020). *Italian D. Lgs. 101/20*. Italian legislative decree on radiation protection.

Mancini, S., Caliendo, E., Guida, M., and Bisceglia, B. (2017). "Preliminary assessment, by means of Radon exhalation rate measurements, of the bio-sustainability of microwave treatment to eliminate

biodeteriogens infesting stone walls of monumental historical buildings". *IOP Conference Series: Materials Science and Engineering* **251**(1), 012026. DOI: 10.1088/1757-899X/251/1/012026.

Morelli, D., Immé, G., Cammisa, S., Catalano, R., Mangano, G., La Delfa, S., and Patanè, G. (2012). "Radioactivity measurements in volcano-tectonic area for geodynamic process study". *European Physical Journal Web of Conferences* **24**, 05009. DOI: 10.1051/epjconf/20122405009.

Navas, A., Soto, J., and Machín, J. (2002). "^{238}U, ^{226}Ra, ^{210}Pb, ^{232}Th and ^{40}K activities in soil profiles of the Flysch sector (Central Spanish Pyrenees)". *Applied Radiation and Isotopes* **57**(4), 579–589. DOI: 10.1016/S0969-8043(02)00131-8.

Omar-Nazir, L., Shi, X., Moller, A., Mousseau, T., Byun, S., Hancock, S., Seymour, C., and Mothersill, C. (2018). "Long-term effects of ionizing radiation after the Chernobyl accident: Possible contribution of historic dose". *Environmental Research* **165**, 55–62. DOI: 10.1016/j.envres.2018.04.005.

Pietrzak, U. and McPhail, D. C. (2004). "Copper accumulation, distribution and fractionation in vineyard soils of Victoria, Australia". *Geoderma* **122**, 151–166. DOI: 10.1016/j.geoderma.2004.01.005.

Righi, S. and Bruzzi, L. (2006). "Natural radioactivity and radon exhalation in building materials used in Italian dwellings". *Journal of Environmental Radioactivity* **88**, 158–170. DOI: 10.1016/j.jenvrad.2006.01.009.

Rodrigues e Silva, C. and Monteiro de Oliveira, F. (2023). "Natural radioactivity in mineral phosphate fertilizers and its impacts on human health: an overview". *Environmental Science and Pollution Research* **30**, 118149–118160. DOI: 10.1007/s11356-023-30467-y.

Rollog, M., Cook, N. J., Guagliardo, P., Ehrig, K. J., and Kilburn, M. (2019). "Radionuclide-bearing minerals in Olympic Dam copper concentrates". *Hydrometallurgy* **190**, 105153. DOI: 10.1016/j.hydromet.2019.105153.

Sabbarese, C., Ambrosino, F., D'Onofrio, A., and Roca, V. (2021). "Radiological characterization of natural building materials from the Campania region (Southern Italy)". *Construction and Building Materials* **268**, 121087. DOI: 10.1016/j.conbuildmat.2020.121087.

Sabol, J. and Weng, P.-S. (1995). *Introduction to Radiation Protection Dosimetry*. World Scientific. DOI: 10.1142/2612.

Stoulos, S., Manolopoulou, M., and Papastefanou, C. (2003). "Assessment of natural radiation exposure and radon exhalation from building materials in Greece". *Journal of Environmental Radioactivity* **69**(3), 225–240. DOI: 10.1016/S0265-931X(03)00081-X.

Torrisi, L., Caridi, F., Margarone, D., and Giuffrida, L. (2008). "Nickel plasma produced by 532-nm and 1064-nm pulsed laser ablation". *Plasma Physics Report* **34**(7), 547–554. DOI: 10.1134/S1063780X08070039.

Tuccimei, P., Mollo, S., Soligo, M., Scarlato, P., and Castelluccio, M. (2015). "Real-time setup to measure radon emission during rock deformation: implications for geochemical surveillance". *Geoscientific Instrumentation, Methods and Data Systems* **4**, 111–119. DOI: 10.5194/gi-4-111-2015.

Tuccimei, P., Moroni, M., and Norcia, D. (2006). "Simultaneous determination of ^{222}Rn and ^{220}Rn exhalation rates from building materials used in Central Italy with accumulation chambers and a continuous solid state alpha detector: Influence of particle size, humidity and precursors concentration". *Applied Radiation and Isotopes* **64**(2), 254–263. DOI: 10.1016/j.apradiso.2005.07.016.

United Nations Scientific Committee on the Effects of Atomic Radiation (2000). *Sources and Effects of Ionizing Radiation*. UNSCEAR Report to the General Assembly, with Scientific Annexes. Volume 1: Sources. United Nations. URL: https://www.unscear.org/unscear/uploads/documents/unscear-reports/UNSCEAR_2000_Report_Vol.I.pdf.

[a] Università degli Studi di Messina,
Dipartimento di Scienze Matematiche e Informatiche, Scienze Fisiche e Scienze della Terra,
Viale F. Stagno d'Alcontres 31, 98166 Messina, Italy

[b] Università degli Studi di Cagliari,
Dipartimento di Fisica,
Cittadella Universitaria di Monserrato, Italy

[c] Università degli Studi di Cagliari,
Dipartimento di Scienze Chimiche e Geologiche,
S.P. Monserrato-Sestu, km 0.700-09042 Monserrato, Italy

[d] Università "Mediterranea di Reggio Calabria",
Dipartimento di Ingegneria dell'Informazione, delle Infrastrutture e dell'Energia Sostenibile (DIIES),
Via Zehender, 89122 Reggio Calabria, Italy

[e] Università degli Studi di Salerno,
Dipartimento di Ingegneria dell'Informazione ed Elettrica e Matematica applicata (DIEM),
Via Giovanni Paolo II, 132-Fisciano (SA), Italy

[f] Università della Calabria,
Dipartimento di Biologia, Ecologia e Scienze della Terra (DiBest),
Via Pietro Bucci, Arcavata di Rende (CS), Italy

[*] To whom correspondence should be addressed | email: fcaridi@unime.it

Communicated 25 November 2024; manuscript received 5 December 2024; published online 25 September 2025